



## UNCERTAINTY IN THE INELASTIC BEHAVIOR OF REINFORCED CONCRETE WALLS DUE TO MATERIAL PROPERTIES

J. A. Gallardo<sup>(1)</sup>, J. C. de la Llera<sup>(2)</sup>, H. Santa María<sup>(3)</sup>, M. Chacón<sup>(4)</sup>

<sup>(1)</sup> PhD student, Pontificia Universidad Católica de Chile (Department of Structural and Geotechnical Engineering; Research Center for Integrated Disaster Risk Management (CIGIDEN), CONICYT/FONDAP/15110017), [jogallardo@uc.cl](mailto:jogallardo@uc.cl)

<sup>(2)</sup> Professor, Pontificia Universidad Católica de Chile (Department of Structural and Geotechnical Engineering; Research Center for Integrated Disaster Risk Management (CIGIDEN), CONICYT/FONDAP/15110017), [jllera@ing.puc.cl](mailto:jllera@ing.puc.cl)

<sup>(3)</sup> Associated professor, Pontificia Universidad Católica de Chile (Department of Structural and Geotechnical Engineering; Research Center for Integrated Disaster Risk Management (CIGIDEN), CONICYT/FONDAP/15110017), [hsm@ing.puc.cl](mailto:hsm@ing.puc.cl)

<sup>(4)</sup> Postdoctoral fellow, Pontificia Universidad Católica de Chile (Department of Structural and Geotechnical Engineering; Research Center for Integrated Disaster Risk Management (CIGIDEN), CONICYT/FONDAP/15110017), [mfchacon@uc.cl](mailto:mfchacon@uc.cl)

### Abstract

Reinforced concrete (RC) walls are structural elements widely used to resist lateral forces in highly seismic countries. Design codes provide minimum requirements to ensure an adequate performance of shear walls during ground motions; however, during recent earthquakes such as the 2010 Maule earthquake in Chile, or the Canterbury, Christchurch 2010 and 2011 earthquakes in New Zealand, some shear walls underwent an unprecedented and somewhat unexpected brittle failure. This fact evidenced that current analysis and design procedures for shear wall buildings do not provide a close representation of the true seismic response of these walls under severe cyclic earthquake loading, which is an imperative in performance-based design. Keeping that in mind, the present research implemented a Nonlinear Finite Element Wall (NLFEW) model, which was validated using parametric analyses. A micro-model using layered-shell elements was selected that uses an effective material model for concrete based on theory of plasticity and continuum damage mechanics. The wall model was validated simulating the behavior of four experimental RC benchmark wall test specimens subjected to quasi-static cyclic loads. Five response parameters were considered to evaluate the accuracy of the model: the initial stiffness, peak base-shear force, peak displacement at the top, ultimate base-shear force, and energy dissipated throughout the cyclic loading. The same parameters were used to quantify the uncertainty generated by the material properties in the global response of each wall. Results show that the model fits very well the experimental tests, and localization of damage is correctly predicted. Moreover, results from sensitivity analyses suggest that the initial stiffness is mainly influenced by variables of concrete in tension; the maximum top displacement (ductility of the element) depends largely on the parameters of concrete in compression; and base-shear forces and dissipated energy are sensitive to the post-yield stiffness of steel reinforcement.

*Keywords: reinforced concrete wall; continuum concrete model; sensitivity analysis; inelastic parametric analysis; benchmark analysis with test specimens.*



## 1. Introduction

Reinforced concrete walls are commonly used as structural elements in countries with high seismicity to resist lateral loads in medium- to high-rise buildings, since they have shown good performance in previous earthquakes. However, during the 2010 Chile earthquake [1] and 2011 New Zealand earthquake [2] a failure with limited ductility was observed, which was characterized by spalling of the concrete cover, buckling of the vertical reinforcement and crushing of the confined concrete at the compression zone (see Fig. 1).



Fig. 1 – Examples of wall damage in buildings; (a) AA-1; (b) AH-2; (c) CM-3; (d) TL-4; (e) PR-6; and (f) RT-8; during the 2010 Chile earthquake [3].

Real data of seismic events is mostly limited to photographs and technical reports, and eventually some aftershock instrumentation of damaged buildings. To partially solve this problem, several experimental campaigns have been carried out by different authors to understand the behavior and failure mechanism of RC walls under seismic loads. Tests have been performed for walls with different geometries and have been used for the calibration of numerical models.

In the last four decades, several numerical models have been developed to simulate the inelastic behavior of RC walls. The models can be grouped according to their modeling approach as macro-models or micro-models. On the one hand, macro-models represent the RC walls by a set of simplified nonlinear elements, which simulate the phenomenological behavior of concrete, steel bars, and their interaction under cyclic loads. On the other hand, micro-models are based generally on Finite Elements (FE). The latter models, where concrete and steel bars are simulated independently with different elements are appropriate to simulate accurately the stress and strain distribution along the entire structural elements at the expense of a higher computational cost.

Based on this information, and considering the failure observed in the buildings (see Fig. 1), micro-models that represent RC walls are necessary. The present research aims to validate a Non-Linear Finite Element Wall (NLFEW) model and analyze the sensitivity of wall responses due to material parameters under cyclic loads. The aim is to compute damage and evaluate uncertainty present in the behavior of the wall. In section 2, the NLFEW model, its element formulation for concrete and steel, and the constitutive model for both materials are summarized. In section 3, the NLFEW model is validated using the experimental results of



four RC walls. Section 4 presents a sensitivity analysis of material parameters in the response of four RC benchmark wall models. Finally, some conclusions are presented for this work.

## 2. Non-linear finite element wall model

The Non-linear Finite Element Wall (NLF EW) model used to reproduce and predict the inelastic behavior of RC Wall elements was implemented in the ANSYS software [4].

### 2.1 Element models

Layered-shell elements (SHELL181) are used to model concrete; each element is defined by four nodes with six degrees of freedom per node. The cross-section is divided in several layers through the thickness, which number depends on the geometry of the section and the reinforcement.

Reinforcement is embedded in the concrete element, and it is modeled as smeared elements, where the steel is distributed within a thin layer (Fig. 2). Each reinforcing layer has a unique orientation, material, and cross-section area, and is simplified as a homogeneous unidirectional membrane (REINF265).

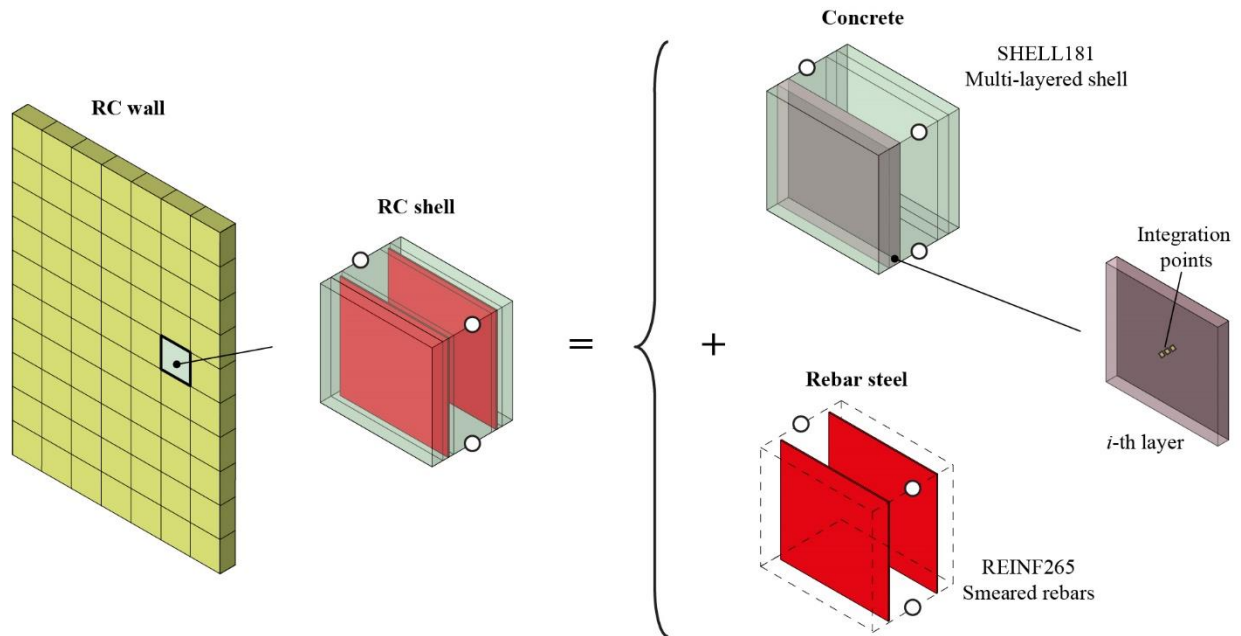


Fig. 2 - Finite element types and their assemblage.

### 2.2 Concrete and steel constitutive models

#### Concrete

The constitutive model proposed by Faria et al. [5] was selected to simulate the concrete behavior, which is based on the theory of plasticity and continuum damage mechanics. The Cauchy stress tensor  $\boldsymbol{\sigma}$  is defined as

$$\boldsymbol{\sigma} := (1 - \omega^+) \bar{\boldsymbol{\sigma}}^+ + (1 - \omega^-) \bar{\boldsymbol{\sigma}}^- \quad (1)$$

where  $\omega^\pm$  are the tension/compression damage variables;  $\boldsymbol{\sigma}^+$  and  $\boldsymbol{\sigma}^-$  are the tensile and compressive components of the effective stress tensor  $\bar{\boldsymbol{\sigma}}$ , respectively. The effective stress tensor  $\bar{\boldsymbol{\sigma}}$  can be written using the theory of plasticity as

$$\bar{\boldsymbol{\sigma}} := \mathbf{C}_0 : \boldsymbol{\varepsilon}^e = \mathbf{C}_0 : (\boldsymbol{\varepsilon} - \boldsymbol{\varepsilon}^p) \quad (2)$$



where  $\mathbf{C}_0$  is the usual fourth-order isotropic linear-elastic stiffness tensor; and  $\boldsymbol{\varepsilon}$ ,  $\boldsymbol{\varepsilon}^e$  and  $\boldsymbol{\varepsilon}^p$  are the total, elastic, and plastic second order strain tensors, respectively, with  $\boldsymbol{\varepsilon} = \boldsymbol{\varepsilon}^e + \boldsymbol{\varepsilon}^p$ . The evolution law of the plastic second order strain tensor  $\boldsymbol{\varepsilon}^p$  is a function of the positive  $B^+$  and negative  $B^-$  plasticity factors.

On the other hand, the damage variables  $\omega^\pm$  are expressed as

$$\omega^\pm = \omega^\pm(r^\pm) \quad (3)$$

with  $r^\pm$  the damage thresholds. The complete description of the model and references can be found elsewhere (e.g. [6]).

Therefore, the input parameters for the concrete model are: (i) the positive  $B^+$  and negative  $B^-$  plasticity factors; and (ii) the uniaxial stress-strain curve. For the unidimensional concrete response in compression, the model selected is the one defined by Saatcioglu and Razvi [7] for confined and unconfined concrete. The parameters to define the stress-strain curve are the maximum compression strength  $f'_c$ ; the modulus of elasticity  $E_c$ ; and the concrete crushing energy in compression  $G_c$ . For confined concrete two additional parameters are defined,  $K_s$  and  $K_e$ , which are the strength and deformation ratios at the peak between the confined concrete and unconfined concrete. For the unidimensional concrete response in tension, the model used is the denominated exponential, where the required parameters are the maximum tensile strength  $f_t$ , and the concrete crushing in tension  $G_t$ . In addition, the model is regularized in tension and compression to avoid mesh-dependent results. Fig. 3 shows the uniaxial concrete model considered.

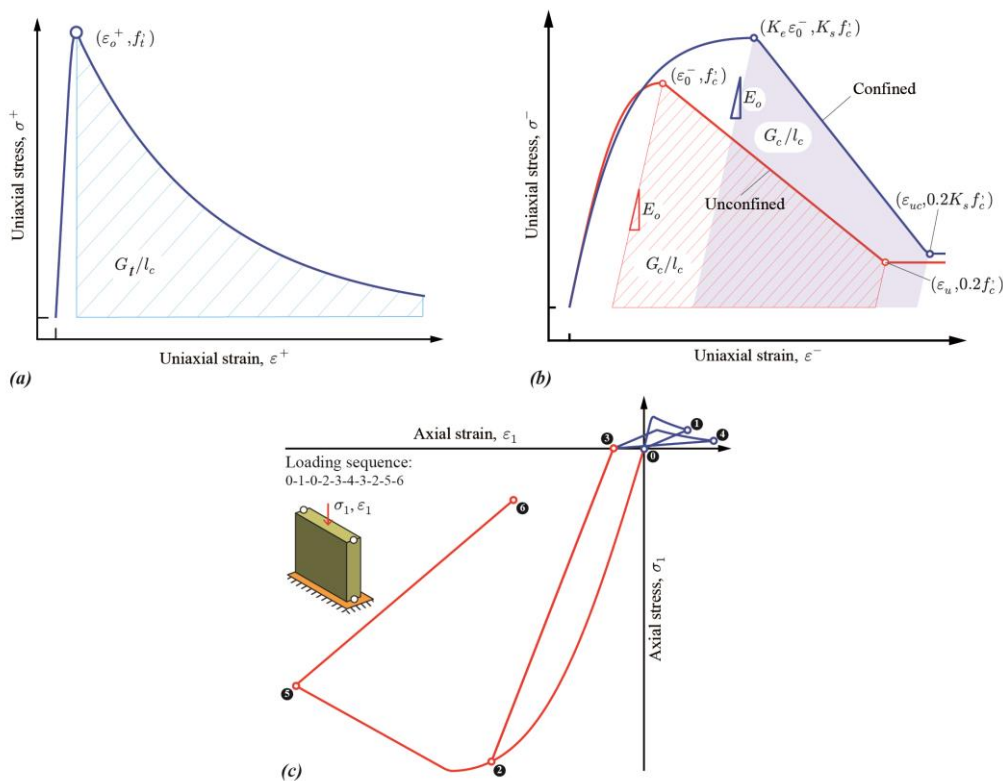


Fig. 3 – Uniaxial concrete model: (a) tension; (b) confined and unconfined in compression; and (c) cyclic loading.



Corners in the uniaxial concrete response have been smoothed by large curvature parabolic transition curves to avoid singularities in the derivatives between different sections of the curve and avoid convergence problems.

### 2.2.2 Steel

The model proposed by Menegotto and Pinto [8] was selected for steel to represent adequately the Bauschinger effect. The anisotropic behavior associated with rebar buckling is implicitly included using a different uniaxial stress law. The parameters for the model are the modulus of elasticity  $E_s$ ; the yield strength in compression  $f_y^-$ ; the yield strength in tension  $f_y^+$ ; the hardening parameter in compression  $b^-(E_p^-/E_s)$ ; and the hardening parameter in tension  $b^+(E_p^+/E_s)$ . Fig. 4 shows schematically the stress-strain constitutive model and the different parameters.

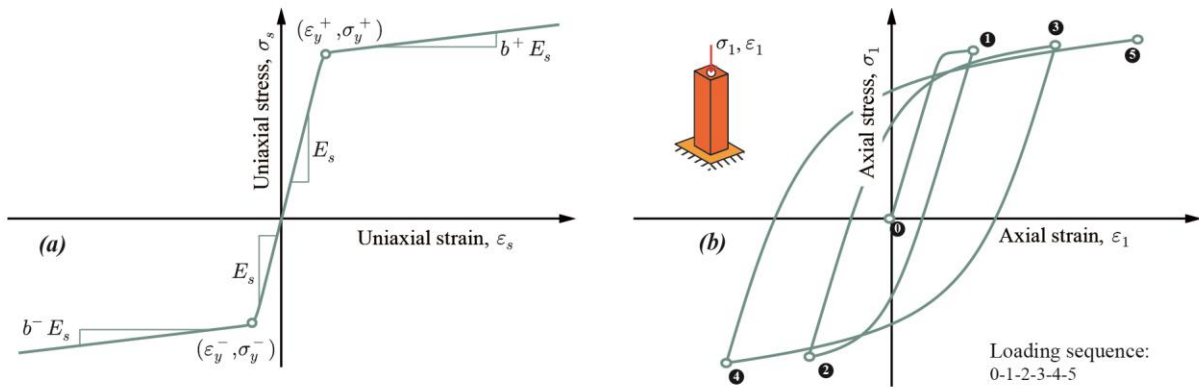


Fig. 4 – Steel stress-strain constitutive model: (a) tension and compression; and (b) cyclic loading.

## 3. Validation of the model

Four RC wall test specimens subjected to quasi-static cyclic loads are used to validate the NLFWE model. The cross sections of the specimens are shown in Fig. 5, while the geometry properties and nominal axial load ratios (ALR) are shown in Table 1, where  $h_w$  is the wall height,  $l_w$  is the wall length,  $t_w$  is the wall thickness,  $\rho_v$  is the vertical reinforcement ratio,  $\rho_h$  is the horizontal reinforcement ratio,  $\rho_b$  is the volumetric reinforcement ratio of the confinement boundary elements, ALR is the ratio between wall axial load and gross section capacity ( $N/A_g f'_c$ ),  $N$  is the wall axial load, and  $A_g$  is the gross cross-section area of the wall.

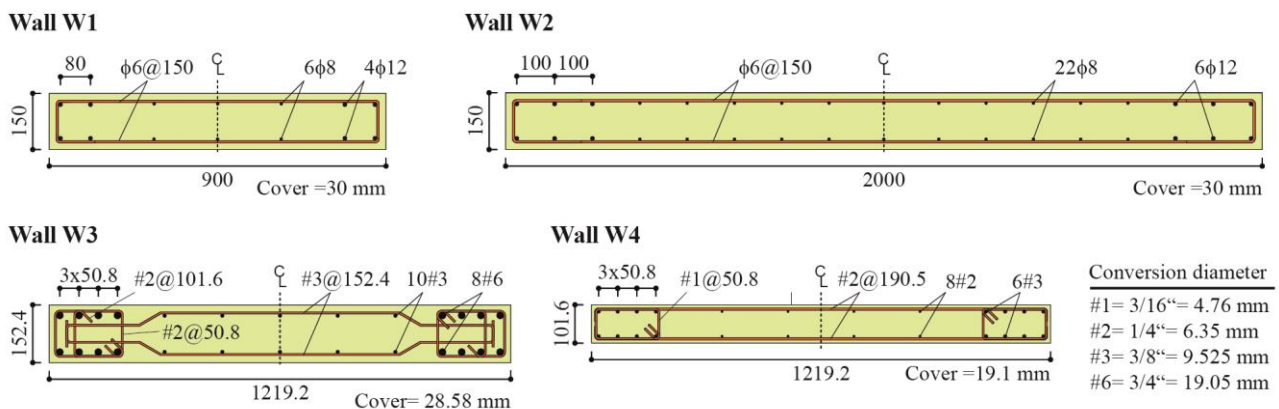


Fig. 5 – Cross-section of RC Wall test specimens: (a) W1 [9]; (b) W2 [10]; (c) W3 [11]; and (d) W4 [12].



Table 1 – General characteristics of RC Wall specimens.

ID	Wall	Author	$h_w$	$l_w$	$t_w$	$l_w/h_w$	$\rho_v$	$\rho_h$	$\rho_b$	ALR
			[cm]	[cm]	[cm]	[-]	[%]	[%]	[%]	[-]
W1	M3	Amon [9]	90	200	15	2.2	0.89	0.25	2.15	0.10
W2	WSH4	Dazio et al. [10]	200	456	15	2.3	0.82	0.25	1.54	0.06
W3	RW-A20-P10-S63	Tran [11]	122	244	15	2.0	2.83	0.61	7.11	0.07
W4	RW2	Thomsen et al. [12]	122	366	10	3.0	1.12	0.33	2.93	0.09

Specimens can be separated into two groups: specimens with a negligible amount of confinement, for which all concrete is considered unconfined (walls *W1* and *W2*); and specimens with confined boundary elements (walls *W3* and *W4*). To evaluate the accuracy of the model and calibrate the material properties, five parameters were considered: (a) initial lateral stiffness  $K_y$ ; (b) peak base shear force  $V_{max}$ ; (c) maximum top lateral displacement  $\Delta_u$ ; (d) ultimate base shear force  $V_u$  (base shear at  $\Delta_u$ ); and (e) energy dissipated under cyclic loading  $E_{dis}$ . The resulting parameters for the calibration of the behavior of concrete are presented in Table 2, the parameters for the different reinforcing bars are presented in Table 3.

Table 2 – Calibrated constitutive parameters for concrete

ID	$E_c$	$f_t$	$f'_c$	$G_c^+$	$G_f^-$	$K_s$	$B^+$	$B^-$
	[GPa]	[MPa]	[MPa]	[N/mm]	[N/mm]	[-]	-	-
W1	26.3	1.375	34.7	$1.75f'_c$	2.0	1.00	0.0	0.2
W2	38.5	1.023	41.7	$2.0f'_c$	2.0	1.00	0.0	0.2
W3	24.2	1.215	42.6	$1.75f'_c$	0.5	1.16	0.0	0.2
W4	21.0	0.001	34.5	$1.75f'_c$	2.0	1.13	0.0	0.2

Table 3 – Calibrated constitutive parameters for steel.

ID	Diameter	$E_s$	$f_y^+$	$f_y^-$	$b^+$	$b^-$
	[mm]	[GPa]	[MPa]	[MPa]	[-]	[-]
W1	6	200	493.0	493.0	0.023	0.023
	8	200	513.0	513.0	0.023	0.023
	12	190	483.0	483.0	0.023	0.023
W2	6	210	518.9	518.9	0.018	0.018
	8	210	583.7	583.7	0.018	0.018
	12	210	576.0	576.0	0.018	0.018
W3	6.4 (#2)	200	308.7	308.7	0.018	0.018
	9.5 (#3)	200	398.7	398.7	0.018	0.018
	19.1 (#6)	200	429.3	429.3	0.018	0.018



W4	4.8 (3/16)	200	390.6	520.8	0.025	0.035
	6.4 (#2)	200	403.2	537.6	0.025	0.035
	9.5 (#3)	200	390.6	520.8	0.025	0.035

Boundary conditions and loading patterns used for the analytical model were identical to those applied in the experimental test. As a first step, axial load was applied, then a horizontal cyclic displacement history was applied. For the mesh, the maximum finite element edge length was 200 mm.

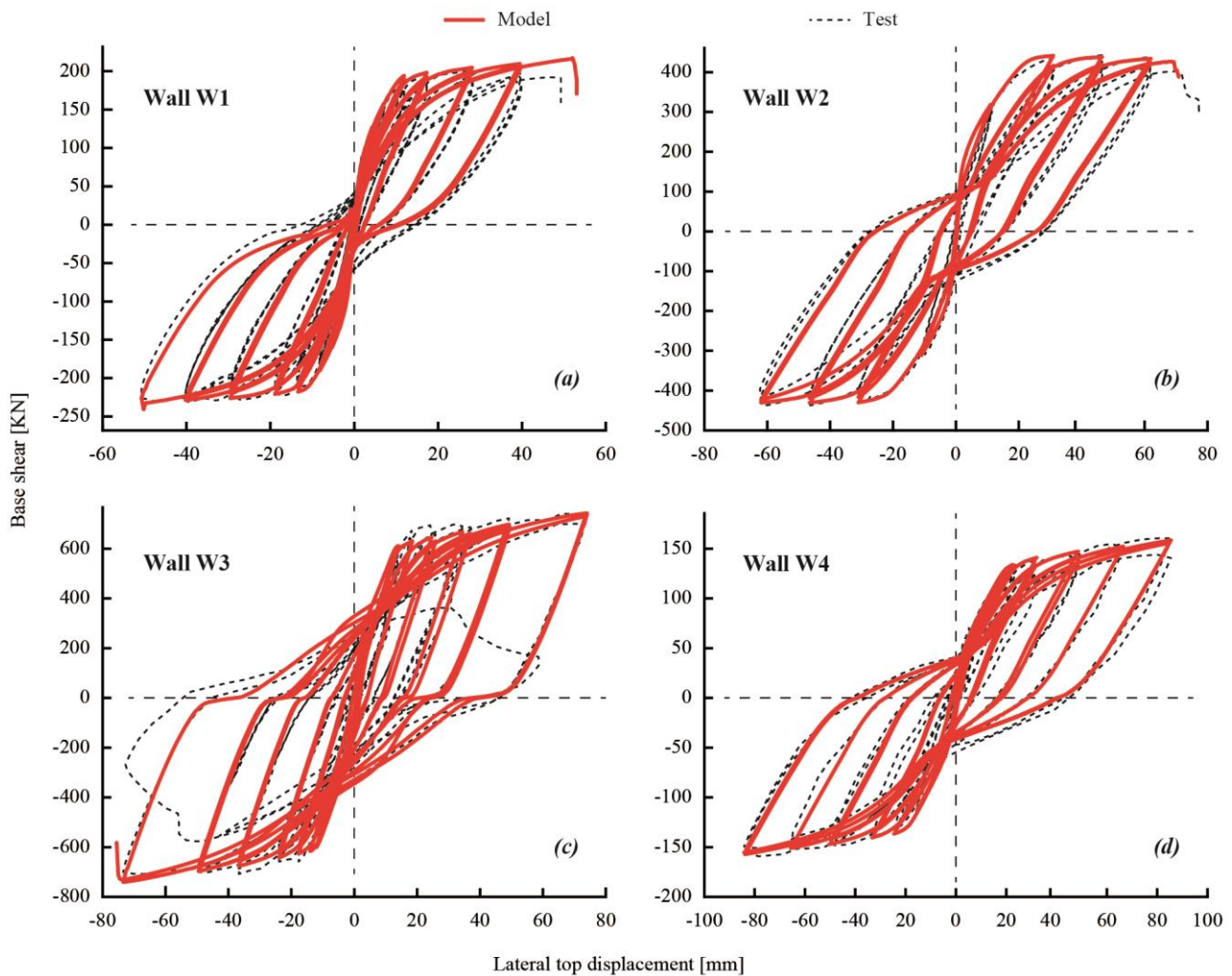


Fig. 6 – Comparison between measured and simulated load-deformation responses using the calibrated parameters: (a) W1; (b) W2; (c) W3; and (d) W4.

Fig. 6 presents a comparison between the measured and simulated load-deformation responses for the four test specimens. It is apparent that for all cases, numerical results fit reasonably well the experimental response. Table 4 compares quantities obtained from the test results, and from the numerical response, and presents the percentage error difference between them. Models of walls *W1* and *W2* predict a higher strength  $V_u$  in 9.4% and 7.6% relative to the experimental test results, respectively. This is due to the fact that the model used does not consider degradation on the materials in each cycle under a constant level of displacement. The same phenomena is present in wall *W3*, where the effect becomes more evident.



Table 4 – Comparison between measured and simulated responses.

ID	$K_y$ [KN/mm]			$V_{max}$ [KN]			$\Delta_u$ [mm]			$V_u$ [KN]			$E_{dis}$ [KJ]		
	Exp	Num	Diff [%]	Exp	Num	Diff [%]	Exp	Num	Diff [%]	Exp	Num	Diff [%]	Exp	Num	Diff [%]
W1	44.1	45.0	+2.0	214	224	+4.5	49.3	52.6	+6.7	192	210	+9.4	65	58	-11.4
W2	73.6	72.2	-1.9	443	441	-0.4	71.7	69.6	-3.0	397	428	+7.6	124	112	-9.2
W3	52.3	60.3	+15.2	740	743	+0.4	74.1	75.0	+1.3	736	711	-3.3	344	396	+15.1
W4	12.3	12.4	+0.4	160	158	-1.2	85.5	85.5	+0.0	160	158	-1.2	67	59	-12.3

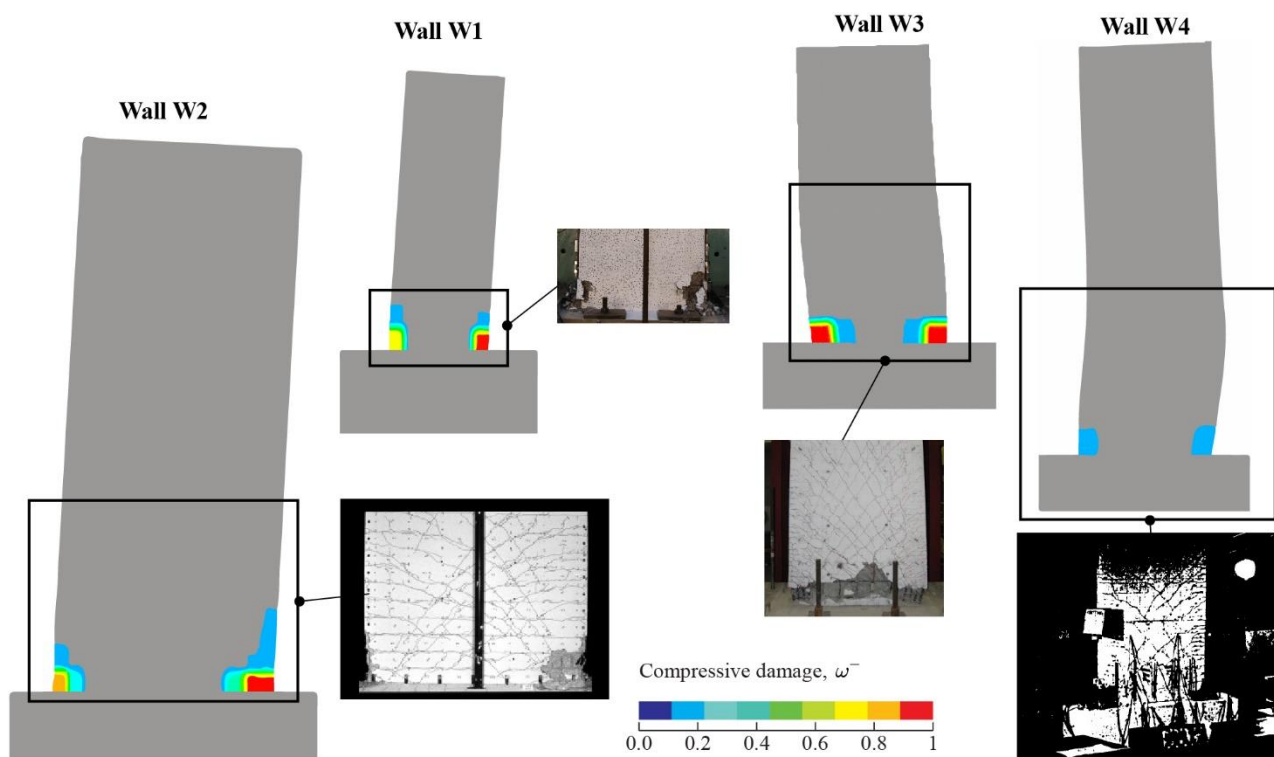
Fig. 7 – Comparison between the predicted and actual damage: contour of compressive damage field  $\omega^-$ , and experimental damage.

Fig. 7 shows the observed and predicted damage at the end of the test. For all walls, the model correctly locates the damage in the specimens, usually localized at the bottom edges of the walls. In walls *W1* and *W2*, damage is localized at the bottom edges, and failure occurs at the right side due to concrete crushing. After crushing the test and simulation are stopped. In spite of the unclear photograph of wall *W4*, damage is apparent at the bottom edges due to concrete crushing. In the experimental test of wall *W3*, failure was induced in both directions, and concrete crushing occurred at both bottom edges with spalling of concrete cover extended throughout the web and the complete bottom section, while in the numerical model, damage is localized at the bottom edges as well, similar to that observed in the experimental test, but damage does not involve the complete section.



#### 4. Sensitivity analysis of the benchmark walls

As a result of the large number of simulation runs for the model calibration, it became apparent that for the NLFEEW model, some material parameters have more influence than others in reproducing the observed response of the actual RC wall. The value of each material parameter is deemed not deterministic and needs to be calibrated to provide an accurate simulation of the wall response.

In order to study the effect produced on the response by each parameter, the wall models of the four benchmark tests were run with different values of the material parameters. The variables considered were the concrete tensile strength  $f_t$  (as a percentage of the concrete compressive strength); the concrete compressive strength  $f'_c$ ; the concrete crushing energy in tension  $G_t$ ; the concrete crushing energy in compression  $G_c$ ; the tension plasticity factor  $B^+$ ; the compression plasticity factor  $B^-$ ; the yield strength in tension and compression of steel,  $f_y^\pm$ ; and the post-yield stiffness of steel  $b^\pm$ . The modulus of elasticity of concrete  $E_c$  was estimated by the ACI equation ( $E_c = 4700\sqrt{f'_c}$  in MPa) for normal weight concrete, while the modulus of elasticity of steel  $E_s$  was taken as the average value of the test results because no significant variability was observed.

Three values were considered in the models for each parameter, selection was done according to suggestions of different researchers. For example, in the case of the  $G_c$ , Pugh et al. [13] recommended a value of  $2.0f'_c$ , while Nakamura and Higai [14] suggested  $1.5f'_c$ . Therefore, the selected values were  $1.5f'_c$ ,  $1.75f'_c$  and  $2.0f'_c$ . The minimum, central, and maximum values of  $f'_c$  and  $f_y$  are those obtained from concrete and steel tests. The complete ranges of values considered for all variables are presented in Table 5.

Table 5 – Material parameter values for sensitivity analysis.

ID	Concrete model									Steel model				
	$f_t$	$f'_c$ [MPa]				$G_t$	$G_c$	$B^+$	$B^-$	$f_y$ [MPa]				$b^\pm$
	[MPa]	W1	W2	W3	W4	[N/mm]	[N/mm]	[-]	[-]	W1	W2	W3	W4	[%]
Minimum	$0.025f'_c$	31.2	36.8	46.6	34.5	0.5	$1.50f'_c$	0.0	0.1	461	505	453	399	1.0
Central	$0.050f'_c$	37.7	40.9	48.6	40.8	1.0	$1.75f'_c$	0.1	0.2	483	519	477	434	3.0
Maximum	$0.100f'_c$	38.1	45.0	51.3	45.7	2.0	$2.0f'_c$	0.2	0.3	496	533	501	456	5.0

Fig. 8 shows the results of the sensitivity analysis, in which all numerical responses are normalized with respect to the responses with the central values and the percentage variations have been obtained. Results show that  $\Delta_u$  is the most sensitive response to the values of the material parameters. The tensile strength of the concrete  $f_t$  is the parameter that produces the largest impact in the initial stiffness of walls, generating a maximum variation of 16% in wall W2; initial stiffness  $K_y$  increases as  $f_t$  increases, this relation is almost linear for all walls analyzed, while  $G_t$ ,  $b^\pm$ ,  $f_y^\pm$  and  $f'_c$  produce a negligible effect. Post-yield stiffness of steel  $b^\pm$  is the parameter that generates the largest variation in the peak base shear, causing a variation of up to 10% in wall W3;  $V_{max}$  increases as  $b^\pm$  increases, while  $G_t$  generates no variation. For the maximum top lateral displacement, the concrete compression strength  $f'_c$  have an important influence, which is reflected in a variation of  $\Delta_u$  of 37% for wall W1; the value of  $\Delta_u$  increases with the value of  $f'_c$  for the four walls, while  $f_t$  does not impact the value of displacement. In the case of the ultimate base shear, results show that  $f'_c$  leads to a variation of up to 10% and post-yield stiffness of steel  $b^\pm$  up to 10% on this response parameter; as parameters increase, the value of ultimate base shear  $V_u$  also increases, which is insensitive to  $f_t$ . The dissipated energy is more influenced by  $b^\pm$  than by any other parameter, with a maximum percentage variation of 15% in wall W1; the dissipated energy by the walls decreases as the value of  $b^\pm$  increases, and being  $f'_c$  the least influential one.

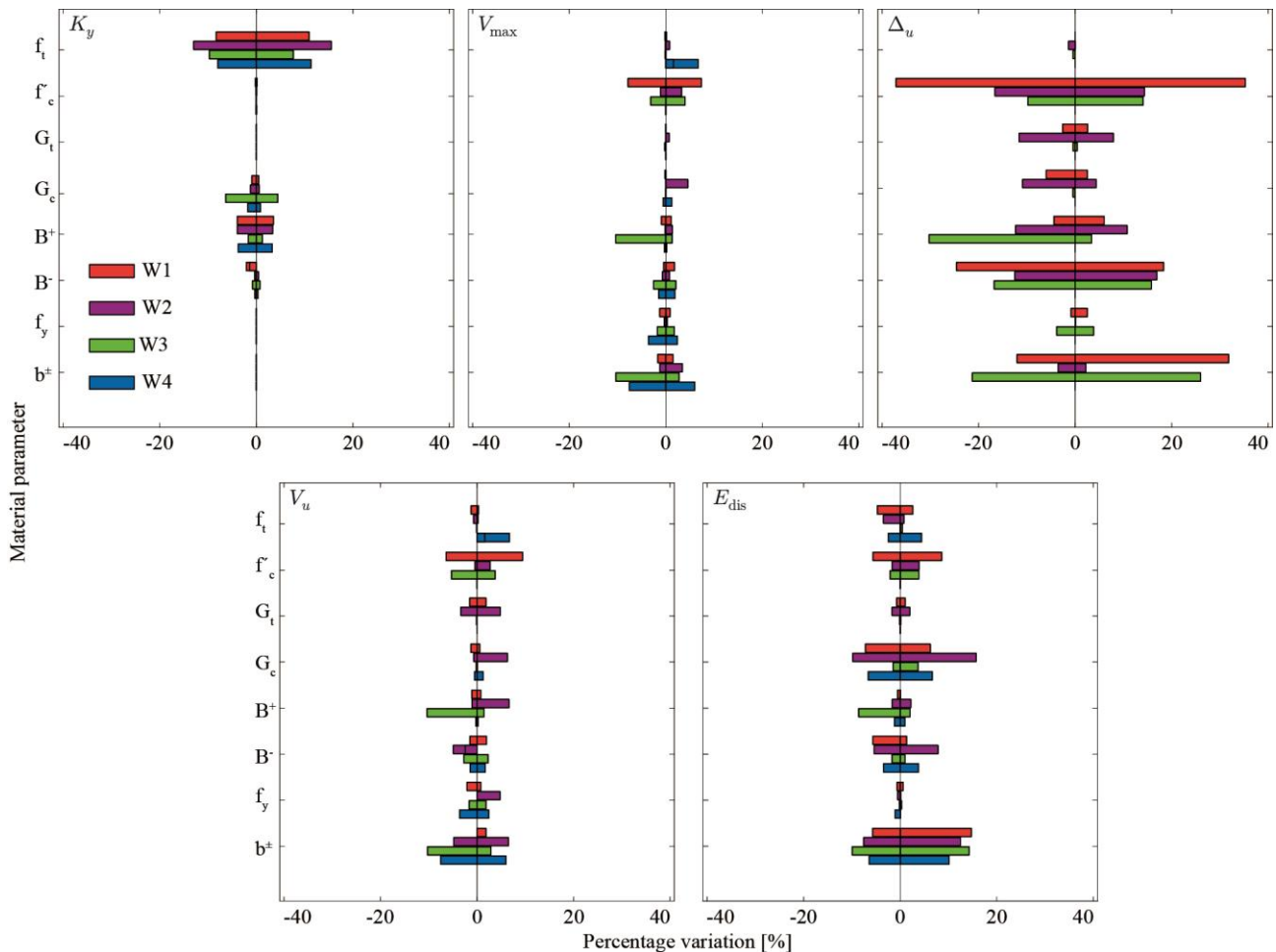


Fig. 8 – Variability of each parameter in the wall response.

## 5. Summary and conclusions

This article presents evidence to validate a NLF EW model to study the inelastic behavior of RC walls under cyclic loading. The wall model reproduces well the quasi-static cyclic benchmark tests of four RC walls, and after the calibration, the influence of each material parameter in the wall response was analyzed. The main conclusions from this study are:

- The NLF EW model was validated using a database of four slender planar tested walls: two with entirely unconfined concrete, and two with confined concrete on the boundary elements. The predicted responses show good agreement with test results for global parameters such as the initial stiffness, peak base shear, peak roof displacement, base shear at peak roof displacement, and dissipated energy, and the same accuracy is achieved for the local responses, such as the concentration of strains and damage location.
- Sensitivity analysis shows that initial stiffness is mainly influenced by parameters of concrete in tension; the maximum lateral displacement and the ductility of the walls depend strongly on the parameters of concrete in compression; and base-shear forces and dissipated energy are significantly affected by the post-yield stiffness of the steel reinforcement.

## 6. Acknowledgements

This research has been sponsored by Ministry of Higher Education, Science, Technology and Innovation of Ecuador (Senescyt), Research Center for Integrated Disaster Risk Management (CIGIDEN), CONICYT /



FONDAP / 15110017, Fondecyt Project SIBER-RISK: Simulation Based Earthquake Risk and Resilience of Interdependent Systems and Networks, CONICYT / FONDECYT / 1170836, and FONDECYT project: Concurso Postdoctorado-2019, CONICYT/ FONDECYT/ 3190680.

## 7. References

- [1] Jünemann R, de La Llera JC, Hube M, Cifuentes L, Kausel E (2015): A statistical analysis of reinforced concrete wall buildings damaged during the 2010, Chile earthquake. *Engineering Structures* **82** 168-185.
- [2] Elwood KJ (2013): Performance of concrete buildings in the 22 february 2011 Christchurch earthquake and implications for canadian codes. *Canadian Journal of Civil Engineering* **40** (3) 759-776.
- [3] Westenenk B, de la Llera JC, Besa JJ, Jünemann R, Moehle J, Lüders C, Inaudi JA, Elwood KJ, Hwang S-J, (2012): Response of reinforced concrete buildings in Concepción during the Maule earthquake. *Earthquake Spectra* **28** (S1) S257-S280.
- [4] ANSYS®: Release 19.2. *ANSYS Inc.*
- [5] Faria R, Cervera J (1998): A strain-based plastic viscous-damage model for massive concrete structures. *International journal of solids and structures* **35** (14) 1533-1558.
- [6] Chacón M, de la Llera JC, Hube M, Calentano D: Review of six 3D continuum stress-strain concrete models – part I: Numerical implementation and consistent notation. *Submitted to International journal of solids and structures.*
- [7] Razvi S, Saatcioglu M (1999): Confinement model for high-strength concrete. *Journal of Structural Engineering* **125** (3) 281-289.
- [8] Menegotto M, Pinto P: Method of analysis for cyclically loaded reinforced concrete plane frames including changes in geometry and non-elastic behavior of elements under combined normal force and bending. *Proceedings. IABSE Symposium on Resistance and Ultimate Deformability of Structures Acted on by Well-Defined Repeated Loads.*
- [9] Amón J (2018): Experimental study of seismic behavior and residual capacity in reinforced concrete slender walls. *Master of Science thesis, Pontificia Universidad Católica de Chile (in Spanish).*
- [10] Dazio A, Beyer K, Bachman H (2009): Quasi-static cyclic tests and plastic hinge analysis of rc structural walls. *Engineering Structures* **31** (7) 1556-1571.
- [11] Tran T (2012): Experimental and analytical studies of moderate aspect ratio reinforced concrete structural walls. *University of California.*
- [12] Thomsen J, Wallace J (2004): Displacement-based design of slender reinforced concrete structural walls – experimental verification. *Journal of structural engineering* **130** (4) 618-630.
- [13] Pugh J, Lowes L, Lehman D (2015): Nonlinear line-element modeling of flexural reinforced concrete walls. *Engineering Structures* **104** 174-192.
- [14] Nakamura H, Higai T (2001): Compressive fracture energy and fracture zone length of concrete. Modeling of inelastic behavior of RC structures under seismic loads 471-487.